

RIS-Assisted D-MIMO for Energy-Efficient 6G Indoor Networks

Akshay Vayal Parambath¹, Jose Flordelis², Venkatesh Tentu¹, Charitha Madapatha¹,
Fredrik Rusek², Erik Bengtsson², Tommy Svensson¹

¹Department of Electrical Engineering, Chalmers University of Technology, Gothenburg, Sweden

²Sony Europe, Lund, Sweden

Abstract—We propose an alternating optimization framework for maximizing energy efficiency (EE) in reconfigurable intelligent surface (RIS) assisted distributed MIMO (D-MIMO) systems under both coherent and non-coherent reception modes. The framework jointly optimizes access point (AP) power allocation and RIS phase configurations to improve EE under per-AP power and signal-to-interference-plus-noise ratio (SINR) constraints. Using majorization-minimization for power allocation together with per-element RIS adaptation, the framework achieves tractable optimization of this non-convex problem. Simulation results for indoor deployments with realistic power-consumption models show that the proposed scheme outperforms equal-power and random-scatterer baselines, with clear EE gains. We evaluate the performance of both reception modes and quantify the impact of RIS phase-shift optimization, RIS controller architectures (centralized vs. per-RIS control), and RIS size, providing design insights for practical RIS-assisted D-MIMO deployments in future 6G networks.

Index Terms—Distributed MIMO, RIS, energy efficiency, spectral efficiency, power allocation, alternating optimization, coherent and non-coherent reception, 6G.

I. INTRODUCTION

APPROACHING the sixth generation (6G) of wireless communications, the applications and use cases are rapidly expanding, leading to a sharp rise in the number of connected devices. Although macro base-station deployments act as the backbone of wireless networks, they often struggle to meet user requirements and fairness as the network grows. To balance these demands, more sophisticated architectures are needed to complement or extend existing infrastructure while ensuring efficient and sustainable operation [1].

Distributed MIMO (D-MIMO), also known as cell-free massive MIMO (CF-mMIMO), has emerged as a promising paradigm, characterized by its adaptability and user-centric (UC) serving capability [2]. In such networks, distributed access points (APs) are dynamically clustered based on user positions, or channel conditions, leveraging either estimated or measured channel state information (CSI). These UC clusters enable flexible AP coordination, improving key performance indicators such as throughput, coverage, and fairness. Despite these advantages, D-MIMO systems still suffer from severe coverage degradation, especially in high-blockage indoor environments [3]. Increasing AP density could mitigate this, but it is neither cost-efficient nor energy-efficient.

This work was supported by the European Commission through the Horizon Europe/JU SNS project Hexa-X-II (Grant Agreement no. 101095759), and the Advanced Digitalization program at the WiTECH Centre DisCouRSe financed by VINNOVA, Chalmers, Ericsson, Qamcom, RISE, SAAB and Volvo Cars.

Even with distributed multi-antenna APs, indoor D-MIMO remains constrained when direct AP-UE links are blocked or subject to severe pathloss, as beamforming cannot bypass obstacles [3]. Reconfigurable intelligent surfaces (RISs) address this by enabling controllable reflections that form alternative paths without deploying additional APs [4]. Unlike network-controlled repeaters that rely on power-hungry amplify-and-forward relaying, RISs are nearly passive arrays of programmable reflecting elements. By intelligently configuring their phase shifts, they align reflected signals with AP-UE links, thereby enhancing signal strength, suppressing interference, and improving link reliability at minimal power cost. With minimal hardware complexity and ease of deployment, RISs complement D-MIMO and serve as an energy-efficient alternative to AP densification in indoor environments.

An additional challenge lies in the non-coherent (NC) reception inherent in D-MIMO systems, where signals from multiple APs may arrive phase-misaligned, disrupting coherent (C) combining and necessitating refined models that jointly optimize RIS configuration and power allocation under both C and NC reception. Here, coherent operation assumes that the serving APs coordinate their transmissions in both time and phase, enabling coherent signal combining at the UE.

Several approaches have attempted to address NC reception in related architectures. For instance, mixed C and NC transmission strategies have been proposed to mitigate NC reception in CF-mMIMO-OFDM systems [5]. In addition, rate-splitting methods [6], have been explored to improve SE in NC conditions. On the EE side, joint AP activation and power allocation for energy-efficient CF-mMIMO networks has been studied in [7]. These works highlight the challenges of NC reception and the importance of SE/EE optimization. However, most existing works either focus on NC reception in CF-mMIMO without RIS [5], [6] or consider EE optimization without jointly accounting for RIS-assisted C and NC reception [7]. Our previous work [8] demonstrated the potential of RIS-assisted D-MIMO for improving indoor coverage and UC clustering. In that study, we showed that dynamic AP clustering combined with RIS assistance can significantly enhance signal-to-interference-plus-noise ratio (SINR), EE, and coverage probability. We further revealed that RISs enable smaller AP clusters to achieve performance comparable to larger clusters, highlighting RIS as a scalable and energy-efficient alternative to AP densification. However, that study did not explicitly address NC reception nor formulated a joint EE optimization framework.

Motivated by these gaps, this paper develops a joint alternating optimization (AO) of RIS phase-shifts and transmit powers to maximize global EE in RIS-assisted D-MIMO systems. Unlike prior works, the proposed framework evaluates the system under both C and NC reception while optimizing transmit power and RIS phase shifts for EE. A detailed power-consumption model is incorporated, including RIS controller and hardware power consumption, and the resulting EE serves as an upper-bound benchmark for practical implementations. Specifically, we incorporate 3GPP Indoor Hotspot (InH) channel models [9]. To address the resulting non-convexity, the proposed AO framework combines majorization-minimization (MM)-based power allocation with RIS phase-shift adaptation. Through simulations, we benchmark the proposed approach against equal-power and random-scatterer RIS baselines, providing insights into the roles of RIS optimization, controller architectures, and RIS size under both reception modes. Overall, the findings show that RIS-assisted D-MIMO effectively balances SE and EE, offering valuable guidance for future 6G wireless networks.

II. SYSTEM MODEL

A. Network Topology and Associations

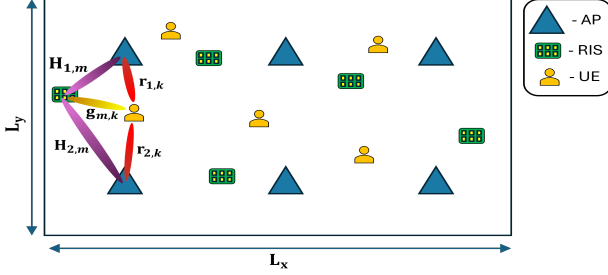


Fig. 1: Illustration of an RIS-assisted D-MIMO downlink system.

We consider a narrowband RIS-aided D-MIMO downlink with L distributed APs, K single-antenna user equipments (UEs), and M RISs as illustrated in Figure 1. The APs are geographically distributed and connected via fronthaul links to a central processing unit (CPU) for UC coordination, joint precoder design, and RIS control. The deployment follows the 3GPP InH model [9], with APs uniformly placed on a grid with spacing D and offset $D/2$ from the walls. The grid size (L_x, L_y) and spacing D are scenario dependent. The system operates at a carrier frequency f_c and bandwidth B . The UEs are distributed following a finite homogeneous Poisson point process (FHPPP). Only a fraction of the K UEs are active per scheduling slot, reflecting realistic indoor traffic loads (e.g., factory environments). Since AP locations are fixed, RIS panels are randomly deployed across the coverage area to support the spatially varying active UEs and provide additional reflected paths in blocked regions. Each AP can serve up to N_{slot} UEs per downlink time slot.

Each active UE $k \in \mathcal{K}_{\text{act}}$ is jointly served by its two strongest APs, forming the cluster $\mathcal{S}_k = \{n_1(k), n_2(k)\} \subseteq \mathcal{L} = \{1, 2, \dots, L\}$. An AP cluster size of two is used to keep the system model tractable while focusing on power allocation and RIS phase optimization. In addition, each UE is assisted

by one RIS selected from $\mathcal{M} = \{1, 2, \dots, M\}$. The AP-UE clustering [2, 10], and UE-RIS association are based on large-scale fading and geometry, so that each UE selects the RIS offering the strongest cascaded AP-RIS-UE channel. The RIS size N_{RIS} determines the passive beamforming gain; under ideal alignment, the reflected-signal power scales with N_{RIS}^2 , thereby improving both SE and EE.

B. Channel Model

We model each AP-UE, and AP-RIS-UE channel according to the 3GPP InH model [9, Table 7.4.1-1, 7.4.2-1], [11] as a Rician fading channel, which accounts for line-of-sight (LoS) probability, pathloss (PL), and shadowing in indoor scenarios. For a generic MIMO channel between a transmitter t with N_t antennas and a receiver r with N_r antennas:

$$\mathbf{H}_{t,r} = \sqrt{\beta_{t,r}} \left(\sqrt{\frac{\kappa_{t,r}}{\kappa_{t,r}+1}} \mathbf{a}_r(\theta_r) \mathbf{a}_t^H(\theta_t) + \sqrt{\frac{1}{\kappa_{t,r}+1}} \mathbf{W}_{t,r} \right), \quad (1)$$

where $\kappa_{t,r}$ is the Rician factor [9, Table 7.5-6], $\beta_{t,r} = G_t G_r 10^{-\text{PL}(d_{3D}, f_c)/10}$ is the large-scale fading (including antenna gains G_t, G_r), $\mathbf{a}_r(\theta_r) \in \mathbb{C}^{N_r \times 1}$ and $\mathbf{a}_t(\theta_t) \in \mathbb{C}^{N_t \times 1}$ are the uniform linear array (ULA) steering vectors at AoA θ_r and AoD θ_t , respectively, and $\mathbf{W}_{t,r} \sim \mathcal{CN}(\mathbf{0}, \mathbf{I}_{N_r} \otimes \mathbf{I}_{N_t})$ is the Rayleigh component. For a ULA with N elements and half-wavelength spacing, the steering vector is given by $\mathbf{a}(\theta) = \frac{1}{\sqrt{N}} [1, e^{j\pi \sin \theta}, \dots, e^{j\pi(N-1) \sin \theta}]^T$, where $\theta \in \{\theta_t, \theta_r\}$.

We denote the AP-RIS channel by $\mathbf{H}_{n,m} \in \mathbb{C}^{N_{\text{RIS}} \times N_{\text{AP}}}$, the RIS-UE channel by $\mathbf{g}_{m,k} \in \mathbb{C}^{N_{\text{RIS}} \times 1}$, and the direct AP-UE channel by $\mathbf{r}_{n,k} \in \mathbb{C}^{1 \times N_{\text{AP}}}$, which will be used in the subsequent signal model formulation. We assume CSI is available at the CPU for the considered indoor scenario with static users, while CSI acquisition is not addressed here. Each RIS m applies a diagonal unit-modulus phase-shift matrix $\Phi_m = \text{diag}(e^{j\theta_{m,1}}, \dots, e^{j\theta_{m,N_{\text{RIS}}}})$, where $\theta_{m,i} \in [0, 2\pi)$.

1) *Coherent Case:* In this case, all distributed APs are assumed to share a common phase reference, thereby achieving network-wide synchronization. This allows their transmitted signals to be combined constructively at the UE, provided that CSI is also well aligned, i.e., the relative phase offsets $\Delta_{n,k}$ between AP n and UE k are effectively zero. The propagation channel between AP n and UE k is

$$\mathbf{h}_{n,k} \triangleq \mathbf{g}_{m_k,k}^H \Phi_{m_k} \mathbf{H}_{n,m_k} + \mathbf{r}_{n,k}, \quad (2)$$

where $\mathbf{r}_{n,k}$ is the direct AP-UE link and the cascaded AP-RIS-UE contributions via the serving RIS m_k are phase-aligned by appropriate choice of Φ_{m_k} . This model represents the best-case system performance, where RIS fully exploit their passive beamforming gain and signals from multiple APs combine coherently at the UE, yielding maximum array gain. While requiring significant synchronization overhead, this coherent case serves as an upper bound against which more practical schemes can be benchmarked.

2) *Non-Coherent Case:* In distributed deployments, however, accurate phase synchronization across transmitting APs is rarely achievable. Denoting the relative phase offset between AP n and UE k as $\Delta_{n,k} = \theta_n - \varphi_k$, each transceiver operates with its own oscillator, resulting in independent random phase

offsets that are not known to the network [5]. The effective channel can be expressed as

$$\tilde{\mathbf{h}}_{n,k} \triangleq e^{j\Delta_{n,k}} \mathbf{h}_{n,k}. \quad (3)$$

Here, the lack of phase alignment prevents coherent combining across APs, reducing the overall array gain and leading to lower SE and EE compared to the coherent case.

C. Signal Model

Let s_k be the unit-power symbol for UE k , and $p_{n,k} \geq 0$ the transmit power from AP n to UE k . The transmit signal at AP n is

$$\mathbf{x}_n = \sum_{j=1}^K \sqrt{p_{n,j}} \mathbf{q}_{n,j} s_j, \quad (4)$$

where $\mathbf{q}_{n,k} \in \mathbb{C}^{N_{\text{AP}} \times 1}$ denotes the precoder at AP n for UE k . The received signal at UE k is

$$y_k^{(\chi)} = \sum_{n \in \mathcal{S}_k} \sqrt{p_{n,k}} \mathbf{h}_{n,k}^{(\chi)} \mathbf{q}_{n,k} s_k + \sum_{j \neq k} \sum_{n \in \mathcal{S}_j} \sqrt{p_{n,j}} \mathbf{h}_{n,k}^{(\chi)} \mathbf{q}_{n,j} s_j + n_k, \quad (5)$$

where the first term represents the desired signal for UE k , the second term accounts for multi-user interference, and $n_k \sim \mathcal{CN}(0, \sigma_k^2)$ denotes the additive Gaussian noise with thermal noise variance σ_k^2 . Here, we use $\chi \in \{\text{C}, \text{NC}\}$ to denote the reception type and write the effective channel as $\mathbf{h}_{n,k}^{(\chi)}$. The instantaneous SE of UE k can be expressed as

$$\text{SE}_k^{(\chi)} = \log_2 \left(1 + \frac{\left| \sum_{n \in \mathcal{S}_k} \sqrt{p_{n,k}} \mathbf{h}_{n,k}^{(\chi)} \mathbf{q}_{n,k} \right|^2}{\sum_{j \neq k} \left| \sum_{n \in \mathcal{S}_j} \sqrt{p_{n,j}} \mathbf{h}_{n,k}^{(\chi)} \mathbf{q}_{n,j} \right|^2 + \sigma_k^2} \right). \quad (6)$$

D. Power-Consumption Model

The total network power consumption in an RIS-assisted D-MIMO system is composed of the transmit power consumed by the power amplifiers (PAs) and several static hardware-related components. Let $\eta_{\text{PA}} \in (0, 1]$ denote the PA efficiency. The dynamic transmit power required to deliver the allocated per-UE powers $\{p_{n,k}\}$ with unit-norm precoders is $P_{\text{PA}} = \frac{1}{\eta_{\text{PA}}} \sum_{n=1}^L \sum_{k=1}^K p_{n,k}$. Following [12], the static power contributions comprises: (i) transceiver-chain power P_{TRxC} , comprising one local oscillator (LO) per AP and the per-antenna RF power at APs and UEs, (ii) fixed per-AP overhead P_{FIX} , and (iii) baseband signal-processing power P_{SP} , scaling with B, L, N_{AP}, K and inversely proportional to computational efficiency $\eta_{\text{AP-c}}$. The RIS hardware also introduces a non-negligible cost, such that the total static power consumption is $P_{\text{static}} = P_{\text{TRxC}} + P_{\text{FIX}} + P_{\text{SP}} + P_{\text{RIS}}$ with $P_{\text{RIS}} = \sum_{m=1}^M (N_{\text{RIS}} P_b + P_{\text{RIS-ctrl}})$, where P_b is the per-element biasing power [4, 13] and $P_{\text{RIS-ctrl}}$ accounts for the controller consumption [14]. For the considered indoor scenario with one RIS per UE ($M = K$), this expression scales linearly with K , and the controller term reduces to a single contribution when centralized RIS control is adopted. The overall network power consumption P_{tot} is the sum of P_{PA} and P_{static} . This model highlights that although RISs introduce only lower P_b , their controller architecture and the AP-side signal-processing complexity can dominate in the P_{static} , thereby strongly influencing the achievable EE.

III. OPTIMIZATION FRAMEWORK

In this section, we first formulate the global EE maximization problem for the RIS-assisted D-MIMO system. We then introduce a compact effective channel representation to simplify the SINR structure and motivate the need for problem reformulation. This leads to an EE objective with power and SINR constraints, forming the basis for the MM-based AO algorithm developed later.

A. Effective Channel-Based Constants

To simplify the SINR analysis in (6), we rewrite the combined AP-RIS-UE channels into compact constants. This isolates desired signal and interference terms in (6), while keeping the optimization problem tractable. For a given UE k , let \mathcal{S}_k denote its serving APs and m_k the associated RIS. The effective channel from AP $n_t(k)$ to UE k , $t \in \{1, 2\}$, combining direct and RIS-reflected paths, is

$$\mathbf{C}_{t,k} = (\mathbf{g}_{m_k,k}^H \mathbf{\Phi}_{m_k} \mathbf{H}_{n_t(k),m_k} + \mathbf{r}_{n_t(k),k}) \mathbf{q}_{n_t(k),k}. \quad (7)$$

Based on these effective channels, the total desired-signal power for UE k can be expressed as

$$A_k(p_{n,k}, \mathbf{\Phi}_{m_k}) = p_{1k} \mathbf{C}_{1k}^{\text{des}} + p_{2k} \mathbf{C}_{2k}^{\text{des}} + \sqrt{p_{1k} p_{2k}} \mathbf{C}_{3k}^{\text{des}}, \quad (8)$$

where $\mathbf{C}_{1k}^{\text{des}} = |\mathbf{C}_{1,k}|^2$, $\mathbf{C}_{2k}^{\text{des}} = |\mathbf{C}_{2,k}|^2$, and $\mathbf{C}_{3k}^{\text{des}} = 2 \Re\{\mathbf{C}_{1,k} \mathbf{C}_{2,k}^*\}$, corresponding to the received power from each AP and their cross-term correlation. Interference from other users is modeled similarly. Let $\mathbf{D}_{\ell j,k}$ denote the effective interfering channel from AP $n_{\ell}(j)$ (serving UE j) to UE k . The total interference-plus-noise power is

$$B_k(p_{n,k}, \mathbf{\Phi}_{m_k}) = \sum_{j \neq k} (p_{1j} \mathbf{C}_{1j,k}^{\text{int}} + p_{2j} \mathbf{C}_{2j,k}^{\text{int}} + \sqrt{p_{1j} p_{2j}} \mathbf{C}_{3j,k}^{\text{int}}) + \sigma_k^2. \quad (9)$$

where $\mathbf{C}_{1j,k}^{\text{int}} = |\mathbf{D}_{1j,k}|^2$, $\mathbf{C}_{2j,k}^{\text{int}} = |\mathbf{D}_{2j,k}|^2$, and $\mathbf{C}_{3j,k}^{\text{int}} = 2 \Re\{\mathbf{D}_{1j,k} \mathbf{D}_{2j,k}^*\}$. The resulting SINR for UE k is

$$\gamma_k(p_{n,k}, \mathbf{\Phi}_{m_k}) = \frac{A_k(p_{n,k}, \mathbf{\Phi}_{m_k})}{B_k(p_{n,k}, \mathbf{\Phi}_{m_k})}. \quad (10)$$

B. Problem Formulation

Using the SINR expression, the global EE maximization problem is formulated as in [7].

$$\begin{aligned} \max_{\{p_{n,k}\}, \{\mathbf{\Phi}_{m_k}\}} \quad & \text{EE}(p_{n,k}, \mathbf{\Phi}_{m_k}) = \frac{B \sum_{k=1}^K \log_2(1 + \gamma_k(p_{n,k}, \mathbf{\Phi}_{m_k}))}{P_{\text{tot}}} \\ \text{s.t.} \quad & p_{n,k} \geq 0, \quad \sum_{k=1}^K p_{n,k} \leq P_n^{\text{max}}, \quad \forall n, k, \\ & \gamma_k(p_{n,k}, \mathbf{\Phi}_{m_k}) \geq \gamma_k^{\text{min}}, \quad \forall k. \end{aligned} \quad (11)$$

The first constraint limits each AP's total transmit power to P_n^{max} , ensuring per-AP power feasibility, while the second enforces γ_k^{min} for each UE. This problem is challenging due to its fractional, non-convex objective and bilinear coupling between power allocation and RIS phases, making conventional convex methods unsuitable. Hence, we adopt an AO strategy, detailed in the next section. Unlike power-minimization problems, the SINR constraints here need not hold with equality since the EE objective inherently balances rate and power.

C. Joint Alternating Optimization Algorithm

We tackle the EE maximization via an AO framework that alternately optimizes (i) power allocation using MM for fixed RIS phases and (ii) RIS phase shifts for fixed powers. Iterative refinement of both variables enables efficient handling of the problem's non-convexity. The compact SINR terms $A_k(p)$ and $B_k(p)$ from (8)-(9) are employed throughout.

1) *MM-Based Power Allocation (fixed Φ_{m_k})*: Given fixed RIS phases, transmit powers are optimized via MM by first convexifying the global EE objective fraction, and then applying a second MM step to approximate the SE term. At iteration t , auxiliary variables $y_k^{(t)}$ are introduced to locally approximate the SINR in (10):

$$y_k^{(t)} \triangleq \sqrt{\frac{A_k(p_{n,k}^{(t)}, \Phi_{m_k})}{B_k(p_{n,k}^{(t)}, \Phi_{m_k})}}, \quad (12)$$

$$\text{SE}_{q_k}^{(t)}(p_{n,k}^{(t)}, \Phi_{m_k}) \triangleq \log_2 \left(1 + 2y_k^{(t)} \sqrt{A_k(p_{n,k}^{(t)}, \Phi_{m_k})} - (y_k^{(t)})^2 B_k(p_{n,k}^{(t)}, \Phi_{m_k}) \right), \quad (13)$$

which locally approximates the SINR. To address the fractional EE objective, a second MM step introduces a global auxiliary ratio $\nu_k^{(t)}$ that linearizes the SE-power coupling per iteration, defined as

$$\nu_k^{(t)} \triangleq \frac{\sum_{k=1}^K \sqrt{B \text{SE}_{q_k}^{(t)}(p_{n,k}^{(t)}, \Phi_{m_k})}}{P_{\text{tot}}^{(t)}}. \quad (14)$$

The ratio $\nu_k^{(t)}$ is then updated from the current power and rate estimates to balance rate and $P_{\text{tot}}^{(t)}$ in each MM iteration.

After the MM reformulation, the objective function remains non-convex due to the bilinear dependence of $B_k(p_{n,k}^{(t)}, \Phi_{m_k})$ on the transmit powers, preventing direct optimization. Thus, it is linearized around the current iterate $p_{n,k}^{(t)}$ using a first-order Taylor approximation, yielding a convex surrogate subproblem [15]. The resulting MM surrogate maximization problem is

$$\begin{aligned} \max_{\{p_{n,k}\}} \quad & 2\nu_k^{(t)} \sum_{k=1}^K \sqrt{B \text{SE}_{q_k}^{(t)}(p_{n,k}^{(t)}, \Phi_{m_k})} - (\nu_k^{(t)})^2 P_{\text{tot}}^{(t)}(p_{n,k}^{(t)}) \\ \text{s.t.} \quad & 2y_k^{(t)} \sqrt{A_k(p_{n,k}^{(t)}, \Phi_{m_k})} - (y_k^{(t)})^2 B_k(p_{n,k}^{(t)}, \Phi_{m_k}) \geq \gamma_k^{\min}, \\ & p_{n,k}^{(t)} \geq 0, \quad \forall k, \quad \sum_{k \in \mathcal{K}_\ell} p_{\ell k}^{(t)} \leq P_\ell^{\max}, \quad \forall \ell, \end{aligned} \quad (15)$$

where $\nu_k^{(t)}$ is the global auxiliary ratio. Solving this convex subproblem yields the updated powers $p_{n,k}^{(t+1)}$, ensuring non-decreasing EE across iterations.

2) *RIS Phase Optimization (fixed powers)*: For a fixed power allocation, each RIS matrix Φ_{m_k} assisting UE k is updated to enhance the desired signal, as shown in Algorithm 1. After each update, the effective channel constants $A_k(\cdot)$ and $B_k(\cdot)$ are recomputed, ensuring consistency with the new RIS configuration. This step exploits the passive beamforming gain of RIS while remaining computationally lightweight.

3) *Outer Loop and Stopping Rule*: The MM-based power allocation and RIS updates alternate until convergence, i.e., until the global EE improvement between two consecutive outer iterations fall below a threshold ϵ , or when the maximum iteration count is reached. This stopping rule ensures

monotonic EE improvement and stable convergence of the AO procedure. The full procedure is outlined in Algorithm 1.

4) *Computational Complexity*: In each outer AO iteration, the algorithm alternates MM-based power allocation and RIS phase optimization. Computing the auxiliary variables $y_k^{(t)}$ and $\nu^{(t)}$ in (12)-(14) has negligible complexity, while the dominant cost arises from solving the convex surrogate problem in (15). In the considered setup, each UE is served by two APs, giving $n = 2K$ real optimization variables. The surrogate problem includes K SINR, N per-AP power, and $2K$ non-negativity constraints, giving $m = 3K + N$ constraints. Using a standard interior-point method, the worst-case per-iteration complexity is $\mathcal{O}((n+m)^{3/2}n^2) = \mathcal{O}((5K+N)^{3/2}(2K)^2)$. For fixed powers, RIS phase optimization uses per-element updates with linear complexity $\mathcal{O}(KM)$ per outer iteration, where M is the number of RIS elements. The total complexity scales linearly with the number of outer AO iterations T_{outer} .

Algorithm 1 AO Framework for EE Maximization

Input: Channel gains; $\{n_1(k), n_2(k)\}$; $\{\gamma_k^{\min}\}$; σ^2 ; $\{P_\ell^{\max}\}$; P_{static} ; B ; max inner/outer iters T, T_{outer} ; K .

Output: Final power allocation $p_{n,k}^{(t+1)}$ and Φ_{m_k} .

- 1: **Initialize:** Set $p_{n,k}^{(0)} = p_{n,k}^0$, $\bar{\text{EE}}^{(0)} = -\infty$
- 2: **for** $n = 1$ to T_{outer} **do** ▷ Outer AO loop
- 3: **—MM-Based Power Optimization (fixed RIS phases)—**
- 4: **for** $t = 0$ to $T - 1$ **do**
- 5: Compute $A_k^{(t)}, B_k^{(t)}, y_k^{(t)}, \text{SE}_{q_k}^{(t)}$, and $\nu^{(t)}$
- 6: Solve surrogate problem in Eq. (15)
- 7: Let $p_{n,k}^{(t+1)} \leftarrow$ optimal solution of surrogate
- 8: Update $p_{n,k}^{(t)} \leftarrow p_{n,k}^{(t+1)}$
- 9: **if** convergence met **then break**
- 10: **end if**
- 11: **end for**
- 12: **—RIS Phase Optimization (fixed powers)—**
- 13: **for** $k = 1$ to K **do**
- 14: Load fixed $\{\mathbf{q}_{1,k}, \mathbf{q}_{2,k}\}$ and $\{p_{1k}^{(t+1)}, p_{2k}^{(t+1)}\}$
- 15: **repeat**
- 16: Compute $\mathbf{g}_k = \mathbf{g}_{1,k}^H, \mathbf{h}_k = \mathbf{H}_{1,1}\mathbf{q}_{1,k} + \mathbf{H}_{2,1}\mathbf{q}_{2,k}$
- 17: Update $\Phi_{m_k} = -\mathcal{L}(\mathbf{g}_k \mathbf{h}_k)$
- 18: Apply phase correction $\theta = \mathcal{L}(\mathbf{r}_{1,k} \mathbf{q}_{1,k})$
- 19: Update cascaded channel with Φ_{m_k}
- 20: **until** convergence
- 21: Save Φ_{m_k} and Update $P_k^{\text{rx}} = \sum_{\ell \in \mathcal{L}_k} p_{\ell k}^{(t+1)} (|\mathbf{r}_{\ell,k} \mathbf{q}_{\ell,k}|^2 + |\mathbf{g}_{1,k} \Phi_{m_k} \mathbf{H}_{\ell,1} \mathbf{q}_{\ell,k}|^2)$
- 22: Recalculate channel gains using updated Φ_{m_k} for UE k
- 23: **end for**
- 24: Compute $\text{EE}^{(n)}$
- 25: **if** $n > 1$ and $\bar{\text{EE}}^{(n)} - \bar{\text{EE}}^{(n-1)} < \epsilon$ **then break** ▷ Converged
- 26: **end if**
- 27: **end for**

IV. PERFORMANCE EVALUATION

A. Simulation Setup

We consider a 300×150 m² indoor area where L APs are uniformly deployed following the 3GPP InH model. The system operates at $f_c = 4$ GHz with $B = 20$ MHz. Each AP ($N_{\text{AP}} = 4$) serves up to $N_{\text{slot}} = 4$ UEs per time slot. A total of $K = 100$ single-antenna UEs are distributed following a FHPPP, with 10% active UEs per slot. Each active UE $k \in \mathcal{K}_{\text{act}}$ is associated with its two strongest APs, forming a UC cluster

$\mathcal{S}_k \subseteq \mathcal{L}$. We deploy $M = 10$ RIS panels, each with N_{RIS} elements, randomly placed in the area, independent of the AP grid. Each UE is assisted by one available RIS applying a diagonal unit-modulus reflection matrix, where each element-wise phase shift $\theta_{m,i} \in [0, 2\pi)$. This RIS control provides an upper bound to practical codebook-based approaches. Each AP's transmit power is limited by P_{ℓ}^{\max} , and σ^2 is obtained from noise power spectral density of $N_0 = -174$ dBm/Hz over B . We set $\gamma_k^{\min} = 0$ to study intrinsic SE-EE behavior without explicit quality-of-service constraints, since enforcing positive SINR targets for all users may lead to infeasibility under the considered deployment and power constraints. The proposed framework is evaluated via Monte Carlo simulations, and remaining parameters are listed in Table I.

TABLE I: Simulation Parameters

Parameter	Value
$L, N_{\text{RIS}}, N_{\text{UE}}, \kappa$	9, 256 (per RIS), 1, 5 dB
Antenna gains $G_{\text{TX}}, G_{\text{RX}}, G_{\text{RIS}}$	5 dB, 2 dB, 4 dB
Shadowing $\chi_{\text{LoS}}, \chi_{\text{NLoS}}$	3 dB, 8.03 dB
$P_{\text{FIX}}, P_{\text{LO}}$	0.875 W, 0.1 W (per AP)
$P_{\text{AP-ant}}, P_{\text{UE-ant}}$	0.2 W, 0.1 W (per antenna)
$\eta_{\text{PA}}, P_{\text{b}}, P_{\text{RIS-ctrl}}, \eta_{\text{AP-c}}$	0.4, 0.997 mW, 4.8 W, 750 Gflop/s

B. Results & Discussion

To show the effectiveness of the proposed joint AO, we evaluate global EE and sum SE under various baselines and system settings. We study the (i) benefits of RIS integration, AP density variations, and baseline comparisons of power allocation and reception models; (ii) gain of joint transmit power and RIS phase optimization; (iii) impact of RIS controller power consumption models; and (iv) effect of RIS size.

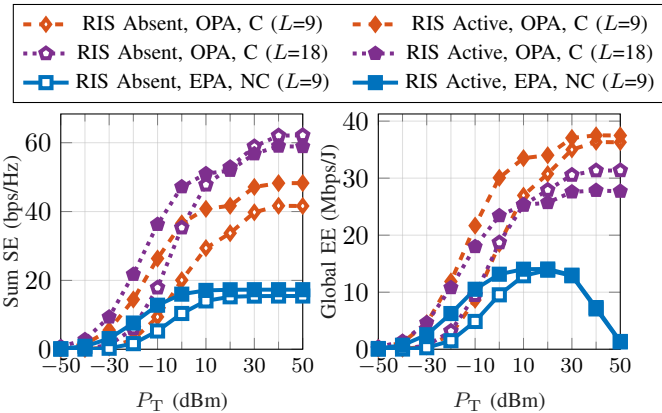


Fig. 2: Sum SE and global EE vs. P_T for a D-MIMO system, comparing benchmarks of RIS integration, and global EE optimization.

1) *SE and EE Behavior*: Figure 2 shows the sum SE and global EE versus P_T ¹. First, optimized power allocation (OPA) consistently outperforms equal power allocation (EPA), particularly at medium and high P_T . The MM-based method adapts transmit power to channel conditions by favoring strong links while avoiding excess power on weaker ones once their SE contribution saturates. As a result, OPA avoids unnecessary transmit power increases after SE saturation, preserving energy

¹Typical indoor AP transmit powers are below 30-35 dBm. Higher transmit power values are considered here only to illustrate EE-SE trends over a wider operating range, as used in Figures 2, 3, and 5.

and sustaining EE gains. In contrast, EPA uniformly distributes P_T across UEs, wasting power on weaker links and causing early EE saturation or decline at high P_T . The EE gap is therefore more pronounced due to inefficient power use.

Second, RIS optimization and AP densification reveal clear performance trade-offs. When RISs are absent, both SE and EE plateau early since UEs rely solely on direct AP-UE links. Activating RISs with optimized phase-shifts (RIS-Opt) i.e., RIS Active, strengthens the effective channel, particularly at moderate P_T , where reflected paths contribute most. Increasing L from 9 to 18 improves SE, but the added APs increase total power consumption, slightly reducing EE. At high P_T , the EE gap narrows between RIS Active and RIS Absent cases with OPA and C combining for $L = 9$, despite higher SE with RIS Active. This indicates that beyond a certain P_T , EE gains from RIS integration diminish as P_{tot} dominates, while higher P_T still yield moderate SE gains from RIS and AP densification.

Third, the reception model significantly affects performance. C combining achieves the highest SE and EE by enabling coherent signal addition across APs. NC combining, while simpler to implement, yields lower performance since signals add only in power domain. Nevertheless, with RIS Active, NC still outperforms the RIS Absent case, showing that RISs remain beneficial even without perfect synchronization.

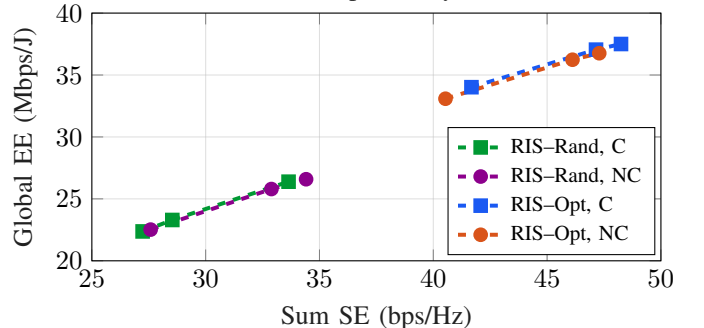


Fig. 3: Global EE vs. sum SE for a RIS-assisted D-MIMO system ($L = 9, N_{\text{RIS}} = 256$) under C and NC reception, comparing RIS-Opt and RIS-Rand with OPA across $P_T \in [20, 40]$ dBm.

2) *Joint Transmit Power and RIS Phase-shift Optimization Significance*: Figure 3 shows the global EE-sum SE tradeoff for RIS-assisted D-MIMO networks with OPA at $P_T \in \{20, 30, 40\}$ dBm. The comparison with random-scatterer (RIS-Rand) baselines under both C and NC reception show that RIS-Opt provides consistent performance gains across all operating points. With RIS-Opt, reflected links constructively combine with direct AP-UE channels, enabling higher SE and translating into improved EE. In contrast, RIS-Rand results in weaker effective channels and lower EE for a given SE. Furthermore, the performance gap between C and NC reception is marginal, indicating that RIS-Opt with OPA remains effective even without coherent combining. However, in both reception models, the relative gain of RIS-Opt over RIS-Rand remains evident. These results highlight that RIS optimization is critical for unlocking the full EE potential of RIS-assisted D-MIMO systems.

3) *RIS Controller Power Consumption Models*: Figure 4 evaluates the impact of RIS controller power at $P_T = 30$ dBm

using optimized transmit power and RIS-Opt. We compare a centralized controller (shared, $P_{\text{RIS-ctrl}} = 4.8\text{W}$) [14] with per-RIS controllers having $P_{\text{RIS-ctrl}} \in \{2.8, 3.8, 4.8\}$ W under C and NC combining. The centralized option attains the highest EE since its overhead is effectively independent of M . For per-RIS control, EE decreases monotonically with $P_{\text{RIS-ctrl}}$ as the static power scales with M . Among per-RIS controllers, the 2.8 W case achieves the highest EE, whereas 3.8-4.8 W yield noticeably lower EE. Across architectures, the C/NC ordering is consistent, but controller power dominates EE, favoring centralized or low-power per-RIS control as M increases.

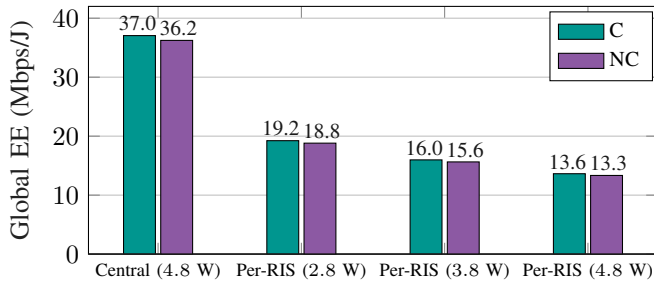


Fig. 4: Global EE of a RIS-aided D-MIMO system ($L = 9$, $N_{\text{RIS}} = 256$) under C and NC combining for centralized and per-RIS control.

4) *Effect of RIS Size:* Figure 5 illustrate that increasing N_{RIS} enhances EE in the low-to-moderate power range due to stronger passive beamforming, though with diminishing returns; the gain from 128 to 256 elements is evident, while the improvement from 256 to 512 elements is modest. As P_{T} increases further, the total power in the EE denominator grows faster than the achievable SE gain, leading to earlier EE saturation. As the RIS panel size increases, the higher static power outweighs the limited additional beamforming gain, resulting in only marginal benefits. At higher P_{T} , the $N_{\text{RIS}} = 256$ case converges with the 128-element curve, while the 512-element case falls slightly below both, indicating reduced energy efficiency for excessively large panels. The C/NC ordering remains consistent, with C combining forming the upper envelope across all considered N_{RIS} configurations.

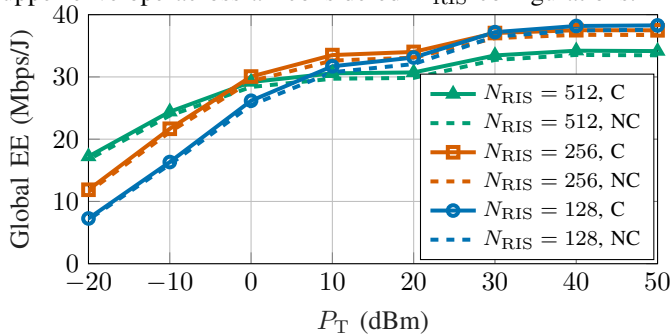


Fig. 5: Global EE vs. P_{T} for a RIS-assisted D-MIMO system with $L = 9$ APs, under C and NC reception using OPA and RIS-Opt.

V. CONCLUSION

This work investigated energy-efficient transmission in RIS-aided D-MIMO systems using a joint AO framework alternating MM-based power allocation and RIS phase-shift optimization. The effective-channel formulation enables efficient surrogate optimization of the non-convex EE problem. Simulation results reveal that OPA outperforms EPA, with

EE peaking at moderate P_{T} . RIS assistance improves both SE and EE, with RIS-Opt consistently outperform RIS-Rand under both combining modes, especially at moderate P_{T} . RIS controller power is critical as centralized control achieves the highest EE, whereas per-RIS control is comparable only at low controller power; higher per-RIS budgets degrade EE as M grows, emphasizing the importance of hardware-aware system design. Scaling N_{RIS} improves EE with diminishing returns, as most gains are captured by medium size panels, and at high P_{T} very large panels add only marginal EE. Finally, C combining forms the upper bound, while NC combining remains effective with RIS phase optimization and adaptive power control.

Overall, the results highlight that both signal processing algorithms and hardware architecture play pivotal roles in determining the EE of RIS-aided D-MIMO networks. Future work may extend the proposed framework to wideband systems to further assess the scalability of energy efficient D-MIMO architectures. Such an extension introduces challenges related to frequency-selective channels, RIS bandwidth limitations, and increased channel estimation and synchronization overhead, which may impact overall energy efficiency.

REFERENCES

- [1] G. Interdonato *et al.*, “Ubiquitous cell-free massive MIMO communications,” *EURASIP J. on Wireless Commun. and Netw.*, vol. 2019, pp. 1–13, 2019.
- [2] E. Björnson and L. Sanguinetti, “Scalable cell-free massive MIMO systems,” *IEEE Trans. Commun.*, vol. 68, no. 7, pp. 4247–4261, 2020.
- [3] M. Di Renzo *et al.*, “Smart radio environments empowered by reconfigurable intelligent surfaces: How it works, state of research, and the road ahead,” *IEEE J. Sel. Areas Commun.*, vol. 38, no. 11, pp. 2450–2525, 2020.
- [4] C. Huang *et al.*, “Reconfigurable intelligent surfaces for energy efficiency in wireless communication,” *IEEE Trans. Wireless Commun.*, vol. 18, no. 8, pp. 4157–4170, 2019.
- [5] G. Li *et al.*, “Asynchronous cell-free massive MIMO-OFDM: Mixed coherent and non-coherent transmissions,” *IEEE Commun. Lett.*, 2024.
- [6] J. Zheng *et al.*, “Asynchronous cell-free massive MIMO with rate-splitting,” *IEEE J. Sel. Areas Commun.*, vol. 41, no. 5, pp. 1366–1382, 2023.
- [7] T. Van Chien *et al.*, “Joint power allocation and load balancing optimization for energy-efficient cell-free massive MIMO networks,” *IEEE Trans. Wireless Commun.*, vol. 19, no. 10, pp. 6798–6812, 2020.
- [8] A. V. Parambath *et al.*, “Integrating reconfigurable intelligent surfaces (riss) into indoor D-MIMO networks for 6G,” in *Proc. IEEE VTC2024-Fall*, 2024, pp. 1–6.
- [9] ETSI, “5G; study on channel model for frequencies from 0.5 to 100 GHz (3GPP TR 38.901 version 16.1.0 release 16),” Tech. Rep., 2020. [Online]. Available: https://www.etsi.org/deliver/etsi_tr/138900_138999/138901/16.01.00_60/tr_138901v160100p.pdf
- [10] Q. Ye *et al.*, “User association and interference management in massive MIMO HetNets,” *IEEE Trans. Commun.*, vol. 64, no. 5, pp. 2049–2065, 2016.
- [11] W. Wang and E. S. Lohan, “Applicability of 3GPP indoor hotspot models to the industrial environments,” in *Proc. IEEE ICL-GNSS*, 2018, pp. 1–5.
- [12] E. Björnson *et al.*, “Massive MIMO networks: Spectral, energy, and hardware efficiency,” *Foundations and Trends® in Signal Processing*, vol. 11, no. 3-4, pp. 154–655, 2017.
- [13] V. Tentu *et al.*, “UAV-enabled hardware-impaired spatially correlated cell-free massive MIMO systems: Analysis and energy efficiency optimization,” *IEEE Trans. Commun.*, vol. 70, no. 4, pp. 2722–2741, 2022.
- [14] J. Wang *et al.*, “Static power consumption modeling and measurement of reconfigurable intelligent surfaces,” in *Proc. IEEE EUSIPCO*, 2023, pp. 890–894.
- [15] S. Boyd and L. Vandenberghe, *Convex Optimization*. Cambridge University Press, 2004. [Online]. Available: https://web.stanford.edu/~boyd/cvxbook/bv_cvxbook.pdf